

*Phthalate Crystals, Advances in X-Ray Analysis* (Plenum, New York, 1970), Vol. 13, p. 373.

<sup>25</sup>K. Siegbahn, C. Nordling, and A. Fahlman, *Electron Spectroscopy for Chemical Analysis* (Institute of Physics, Uppsala, Sweden, 1968).

<sup>26</sup>B. L. Henke, *Norelco Reporter* **14**, 554 (1967).

<sup>27</sup>T. B. Kirby, Masters thesis (New Mexico State University, 1970) (unpublished).

<sup>28</sup>H. Schnopper, *The Argon K Absorption Edge: Two Crystal X-Ray Spectrometry* (Material Science Center, Cornell Univ., Ithaca, N. Y., 1962), p. 44.

<sup>29</sup>In this method the experimental curve is chosen as a first approximation to the corrected isochromat. It is smeared with the normalized monochromator window function, and then the difference between the experimental curve and the smeared curve is added to the experimental curve to produce a second approximation to the "true" isochromat. This process is repeated until the desired convergence of the smeared curve to the experimental curve is achieved. In the smearing operation, a point on the smeared curve is given by the convolution of the original curve with the monochromator window function when the latter is so situated that its peak falls at the

energy of the point.

<sup>30</sup>H. Merz and K. Ulmer, *Z. Physik* **210**, 92 (1968).

<sup>31</sup>Y. Cauchois and C. Bonnelle, in Ref. 20.

<sup>32</sup>S. Hanzély and R. J. Liefeld, *An L-Series-X-Ray Spectroscopic Study of the Valence Bands in Iron, Cobalt, Nickel, Copper, and Zinc*, Natl. Bur. Std. (U.S.) Publ. No. 323 (U.S. GPO, Washington, D. C., 1971).

<sup>33</sup>S. Hanzély, Ph.D. dissertation (New Mexico State University, 1970) (unpublished).

<sup>34</sup>R. L. Park and J. E. Houston, *Phys. Rev. B* **6**, 1073 (1972).

<sup>35</sup>S. Hüfner, G. K. Wertheim, R. L. Cohen, and J. H. Wernick, *Phys. Rev. Letters* **28**, 488 (1972).

<sup>36</sup>The uncorrected isochromat for copper obtained here (Fig. 4) is in good agreement with one shown in Ref. 13.

<sup>37</sup>E. C. Snow and J. T. Waber, *Acta Met.* **17**, 623 (1969).

<sup>38</sup>D. A. Papaconstantopoulos, J. R. Anderson, and J. W. McCaffrey, *Phys. Rev. B* **5**, 1214 (1972).

<sup>39</sup>J. O. Dimmock, in *Solid State Physics* (Academic, New York, 1971), Vol. 26, p. 184.

<sup>40</sup>B. L. Henke and R. E. Lent, *Advances in X-Ray Analysis* (Plenum, New York, 1969), Vol. 12, p. 480.

## Influence of Grain Boundaries and Lattice Defects on the Optical Properties of Some Metals

Ola Hunderi\*

*Physics Department, Victoria University, Wellington, New Zealand*

(Received 25 September 1972)

A simple theory is developed to study the influence of grain boundaries and lattice defects on the optical properties of metals. It is shown that even for well-annealed thin-film samples the influence of grain boundaries on the optical properties is not negligible when the reflectivity is high. The model is used to show that the anomalous absorptivity in alkali-metal films evaporated onto cold substrates recently reported by Palmer and Schnatterly is due predominantly to a plasma resonance in the grain boundaries. It is also found that the non-Drude behavior of Ag in the visible and the supplementary absorption in poorly crystallized Au films, observed by Devant and Theye, most probably is due to such plasma resonances in the grain boundaries.

### I. INTRODUCTION

Optical measurements have been used extensively as a tool for investigating the electronic structure of matter for many decades—and the interest in such measurements has been particularly strong in recent years. These measurements have been helpful in establishing values of parameters used in band-structure calculations.

The optical properties are often sensitive to the sample structure. Two types of samples are used in optical measurements: bulk crystals (often single crystals) and evaporated films. The former, prepared by mechanical- and electrical-polishing techniques, will always have scratches, bumps, and pits in the surface and these will influence the measurements. These types of sample imperfections have been studied extensively over the last few

years. Thin evaporated films consist of small crystallites of diameter generally less than  $1 \mu$ . These crystallites are often randomly oriented; there are dislocations, lattice vacancies, and other defects along the grain boundaries. Little has been done to study the influence of the crystallite structure on the optical properties but, as shown by Devant and Theye,<sup>1</sup> the optical properties may depend dramatically upon the sample structure.

In this paper the influence of grain boundaries on the optical properties of some metals is examined using a simple model. In Sec. II the model is outlined and in Sec. III a simple theory is presented. In Sec. IV the general effects caused by grain boundaries and sample imperfections for the metals K, Ag, and Au are discussed. An attempt is made to estimate the minimum grain size necessary to give essentially bulk conditions. What effects

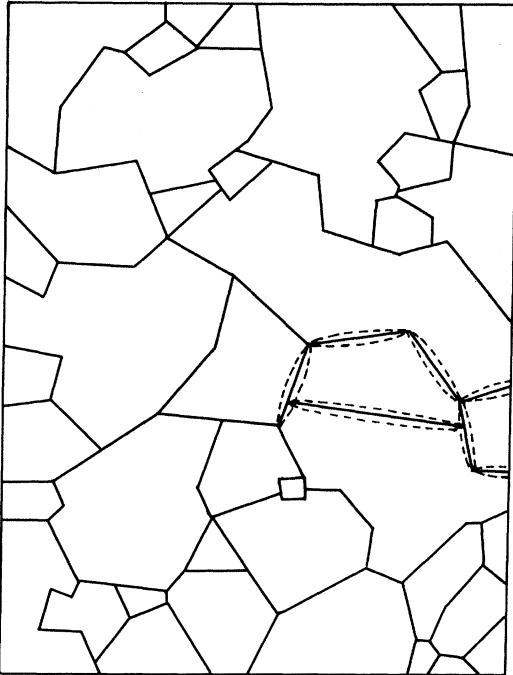


FIG. 1. Grain structure of a typical thin-film sample. The ellipsoids used in the model calculations are indicated along a few grain boundaries.

might be expected in samples which have very small grains and large amounts of crystal imperfections are also studied. Finally, in Sec. V it is shown that several effects observed by previous authors and hitherto unexplained can be understood in terms of sample imperfections.

## II. THE MODEL

The model taken for the grain boundaries was a disordered array of polarizable scatterers embedded in a homogeneous medium. The grain boundaries were represented as flat ellipsoidal disks with a dielectric constant different from that of the bulk material. The ellipsoids were embedded with their short axis parallel to the sample surface, but had, apart from that, a random orientation. The thickness of the disks was taken to be  $10 \text{ \AA}$ ; i. e., a few times a typical screening distance. The other dimensions were determined by the average grain size in the material. This can vary from typically a hundred angstroms along the sample surface to a few thousand angstroms, depending upon preparation method and sample quality. The depth of the ellipsoids was taken to be a few hundred angstroms (i. e., of the order of a typical skin depth). This is illustrated in Fig. 1 which shows the crystallite structure of a typical thin-film sample. A few of the ellipsoids representing the grain boundaries in the model are drawn in as illustration.

The dielectric constant of the material in the ellipsoids was assumed to differ from the bulk dielectric constant only in the Drude part. The grain boundary provides additional scattering, hence the lifetime of electrons near the boundary will be shorter than in the bulk material. It is not known if the scattering by the grain boundary is completely diffuse or not. Throughout the calculations it was therefore arbitrarily assumed that about half of the electrons were diffusely scattered, the rest being specularly scattered by the boundary or transmitted without scattering.

Dislocations, voids, and other defects along the grain boundaries will make the electron density different from that of the bulk material—hence the plasma frequency of the material in the ellipsoids was assumed to be different from the bulk-material plasma frequency. This plasma frequency will vary from grain to grain and the variation was represented by a distribution function of plasma frequencies  $g(\omega_p^2)$  which was taken to be Gaussian. For lack of knowledge, the Gaussian was always centered at the plasma frequency of the bulk material and its width is a measure of how large density variations are found along the grain boundaries. Such density variations are illustrated in Fig. 2 which shows the lattice structure near a grain boundary.<sup>2</sup> Small voids in the lattice still have a finite *electron* density. If the smallest dimension of a void is only a few angstroms, the electron density may easily be 25% of the average electron density. (This has been ignored in a recent paper by Galeener<sup>3</sup> treating the resonant absorption in microscopic voids in amorphous Ge.) Such voids represent the largest variation of the electron density

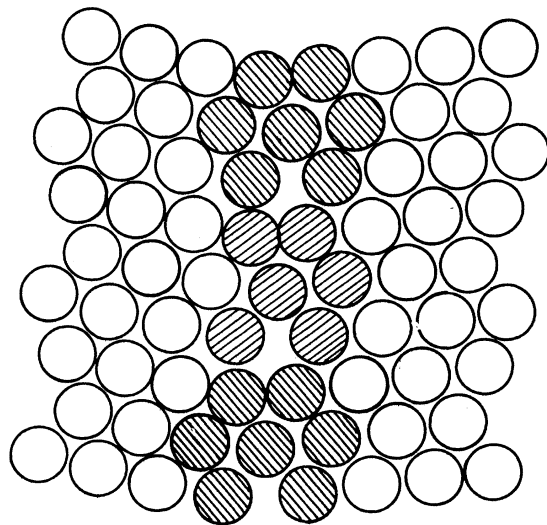


FIG. 2. Possible lattice structure near a grain boundary.

and in the calculations the variation of the plasma frequency was restricted to a region which was chosen to be  $\pm \frac{1}{2} \omega_p$  around the plasma frequency of the bulk material; i. e., the Gaussian distribution function was cut off at  $\omega_p \pm \frac{1}{2} \omega_p$ . The dielectric constant of the material representing the grain boundary was then obtained by changing the Drude part of the dielectric constant of the bulk material to that appropriate to the plasmon frequency and lifetime of electrons near the grain boundary. The interband part of the dielectric constant was not changed. Since the electron density changes, the interband part will also obviously change. Hence the results apply mostly to the intraband region. As will be shown later, though, this is where one finds the largest and most prominent effects.

The ellipsoids were assumed to have sharp boundaries. This was probably not too serious an assumption. A continuously varying density in the ellipsoids would broaden resonance structures but the main effects would remain.

The results obtained with this model were not particular to the choice of model. Representing the grain boundaries as a thin spherical shell of grain-boundary material in an otherwise uniform medium gave nearly identical results as those presented below as long as the thickness of the shell was much smaller than the diameter of the grain.

### III. THEORY

The theory presented here is an extension of the theory developed previously for the reflectivity of a model rough surface by Hunderi and Beaglehole.<sup>4</sup> There we considered a model with small spheres located just above the surface of a metal. Here one considers a random array of ellipsoids embedded in the material below the surface.

If a polarizable scatterer is illuminated by a plane wave propagating along the  $z$  direction in a medium of dielectric constant  $\epsilon$  (refractive index  $N$ ),

$$u_0 = e^{-iNkz + i\omega t}, \quad (1)$$

the scattered wave is a spherical outgoing wave,

$$u = S(\theta, \varphi) e^{-ikNr + i\omega t} / Nkr. \quad (2)$$

Assume the half-space  $z > 0$  filled with particles which are all identical and all identically oriented. Summing over the scattered fields from all scatterers, the total amplitude of the backscattered wave becomes, neglecting near-field effects,<sup>5</sup>

$$u = u_0(\pi/iN^3k^3)\rho S(\pi). \quad (3)$$

Here  $\rho$  is the density of scatterers. This is the usual Fresnel expression modified to account for the absorption by the surrounding medium which gives an extra factor  $1/2Ni$ .

To first order the amplitude function  $S(\pi)$  is given

by the dipole approximation<sup>5</sup>

$$S(\pi) = ik^3 N^3 \alpha, \quad (4)$$

where  $\alpha$  is the electrostatic polarizability of the particle. Inserting this into (3) one obtains

$$u = -u_0 \pi \alpha \rho. \quad (5)$$

For nonspherical particles,  $\alpha$  is polarization dependent. For light polarized along one of the major axes of an ellipsoid,  $\alpha$  is determined by the depolarization factor  $L_i$  along that axis and is given by<sup>5</sup>

$$\alpha_i = \frac{V}{4\pi} \frac{\epsilon_a - \epsilon}{\epsilon + (\epsilon_a - \epsilon)L_i}. \quad (6)$$

$V$  is the volume of the ellipsoid and  $\epsilon_a$  is the dielectric constant of the material in the ellipsoid. For randomly oriented ellipsoids, Eq. (5) takes the form

$$u = -u_0 \frac{1}{4} V_f \alpha_f = -u_0 \frac{1}{4} V_f \times \frac{1}{2} \left( \frac{\epsilon_a - \epsilon}{\epsilon + (\epsilon_a - \epsilon)L_1} + \frac{\epsilon_a - \epsilon}{\epsilon + (\epsilon_a - \epsilon)L_2} \right). \quad (7)$$

$L_1$  and  $L_2$  are the depolarization factors for light polarized along the two major axes parallel to the sample surface.  $V_f$  is the fractional volume of the sample occupied by the ellipsoids. Note that one major axis of the ellipsoids was assumed always to be oriented normally to the sample surface and thus along the direction of the incident light.

When light is incident normally upon a sample containing a fractional volume  $V_f$  of such ellipsoids, the reflectivity is found by summing all the reflected waves. Taking multiple reflections between the scatterers and the sample surface into account, but neglecting multiple scatterings between the ellipsoids, one obtains for the reflectivity  $R$ ,

$$R = |(r + r_s)/(1 + r_s r)|^2, \quad (8)$$

with  $r = (1 - N)/(1 + N)$  and  $r_s = -\frac{1}{4} V_f \alpha_f$ . Thus

$$R = R_0 \left| \frac{1 - \frac{1}{4} V_f \alpha_f [(1 + N)/(1 - N)]}{1 - \frac{1}{4} V_f \alpha_f [(1 - N)/(1 + N)]} \right|^2, \quad (9)$$

which to first order gives for the reflectivity

$$R = R_0 (1 - 2 \operatorname{Re}\{V_f \alpha_f [N/(1 - N^2)]\}). \quad (10)$$

Here  $R_0$  is the reflectivity of the sample in the absence of scatterers.

Equation (9) can easily be inverted to give the effective dielectric constant  $\epsilon_g$ ,

$$\epsilon_g = \epsilon \left[ (1 + \frac{1}{4} V_f \alpha_f) / (1 - \frac{1}{4} V_f \alpha_f) \right]^2. \quad (11)$$

To first order this is the same as the Sillars-Clausius-Mosotti equation<sup>6</sup>

$$\epsilon_g = \epsilon(1 + V_f \alpha_f), \quad (12)$$

but the author feels that Eq. (9) is a better approximation to the reflectivity in the high-reflectivity region since it takes multiple scatterings between the sample surface and the ellipsoids into account.

Multiple scatterings between the ellipsoids can be taken into account by considering one ellipsoid to be in an effective field generated by all the other ellipsoids.<sup>7</sup>  $\alpha_f$  in (11) would then be given by

$$\alpha_f = \frac{1}{2} \left( \frac{\epsilon_a - \epsilon_g}{\epsilon_g + (\epsilon_a - \epsilon_g)L_1} + \frac{\epsilon_a - \epsilon_g}{\epsilon_g + (\epsilon_a - \epsilon_g)L_2} \right), \quad (13)$$

and  $\epsilon_g$  in Eq. (11) could be calculated by successive approximations.

When one has more than one type of particle, the term  $V_f \alpha_f$  is substituted by a sum  $V_f \sum_i g_f^i \alpha_f^i$ .  $V_f$  is the total fractional volume occupied by ellipsoids,  $g_f^i$  is the fraction of ellipsoids of type  $i$  and  $\alpha_f^i$  is the polarizability of particles of type  $i$ .

Expression (9) has been used to calculate the influence of grain boundaries, represented as flat ellipsoidal disks, on the reflectivity of some noble metals (Au and Ag) and some alkali metals (Na and K). One has thus neglected multiple scatterings between the ellipsoids. The results are discussed in Sec. IV

In these calculations, all the ellipsoids representing the grain boundaries in a particular sample were assumed to be of the same shape; i. e., have the same  $L_1$  and  $L_2$ . As discussed in Sec. II, the dielectric constant of the material in the particles varied according to the distribution function of plasmon frequencies  $g(\omega_p^b)$ .

#### IV. GENERAL RESULTS

In this section some general results for the reflectivity change of samples containing grain boundaries and lattice imperfections are presented after first discussing the parameters entering into the calculations.

There are three independent parameters in these calculations: the average grain size in the sample, the lifetime, and the width  $W$  of the distribution of plasmon frequencies for electrons in the grain-boundary material. If the average grain size is given, the depolarization factors  $L_1$  and  $L_2$  and the volume fraction  $V_f$  are also determined, since the short axis of the grain-boundary ellipsoids was kept constant (10 Å).

Flat ellipsoidal disks have a depolarization factor  $L_1 = 1$  for a field perpendicular to their plane and  $L_2 = 0$  for a field in their plane. Strongly elongated spheroids (needles) have  $L_1 = 0$  along their length and  $L_2 = \frac{1}{2}$  across. Spheres have  $L_1 = L_2 = \frac{1}{3}$ . Ellipsoids which are 10 Å wide, 500 Å long, and 200 Å deep have  $L_1 = 0.93$  for a field perpendicular to their plane and  $L_2 = 0.02$  along their longest axis.

Round disks 10 Å thick and 100 Å in diameter have  $L_1 = 0.84$  and  $L_2 = 0.08$ . A long ellipsoidal disk 10 Å thick, 200 Å deep, with a length larger than 2000 Å has  $L_1 = 0.95$  for a field along its short axis and  $L_2 \approx 0$  along the longer axis. The values of  $L_1$  and  $L_2$  have been calculated using the approximate formulas in Ref. 5. It is interesting to notice that a narrow range of values of the depolarization factors ( $0.8 < L_1 < 0.95$ ,  $0.0 < L_2 < 0.1$ ) covers all reasonable shapes of ellipsoids representing the grain boundaries.

The volume fraction  $V_f$  is inversely proportional to the average grain diameter.  $V_f$  is about 0.2 for an average grain diameter of 100 Å and 0.01 for a grain diameter of 2000 Å. The typical volume fraction was obtained for a well-annealed gold film from an electron micrograph of the film.<sup>1</sup> With 10-Å-thick disks along the grain boundaries the fractional volume occupied by grain-boundary material was found to be 0.01.

Throughout these calculations the mean lifetime of electrons in the grain-boundary ellipsoids was taken to be  $2.2 \times 10^{-15}$  sec. For gold this corresponds to a mean free path of 30 Å. If a fraction  $p$  of the electrons is diffusely scattered by the grain boundary, 30-Å mean free path corresponds to  $p \approx 0.5$ .

The calculations were done for three values of  $W$ . These were  $W \approx 0$ ,  $\frac{1}{4}\omega_p$ , and  $\frac{1}{2}\omega_p$ , respectively. Since the variations of the plasma frequency were restricted to the range  $\pm \frac{1}{2}\omega_p$  around  $\omega_p$ , a width of  $\frac{1}{2}\omega_p$  may seem unreasonable. It corresponds to a sample with a large amount of lattice voids.

Smoothing out the sharp cutoff of the distribution function, however, or including larger variations in the plasma frequency near the grain boundaries, has no effect on the general conclusions which we draw from these calculations.

##### A. Alkali Metals

In Fig. 3 the relative change in the reflectivity,  $\Delta R/R_0$ , due to grain boundaries is plotted versus wavelength for a potassium sample.  $\Delta R$  is equal to  $R - R_0$ , where  $R$  and  $R_0$  are the reflectivity with and without grain boundaries, respectively. The parameters  $L_1$  and  $L_2$  are characteristic of a well-annealed sample and the volume fraction is nominally set at 0.01. For the dielectric constant the values recently published by Palmer *et al.*<sup>8</sup> (which in fact are the values for a sample with grain boundaries) were used. We see a broad resonance for  $W = 2.0$  eV and  $W = 1.0$  eV in the region 0.35–0.60  $\mu$  with a weak additional structure at 0.35  $\mu$ . The maximum change in reflectivity shifts to lower wavelengths as  $W$  is decreased and approaches the plasma frequency  $\omega_p$  when  $W$  approaches zero. In Figs. 4 and 5 the relative change in reflectivity is plotted versus wavelength for a potassium sample

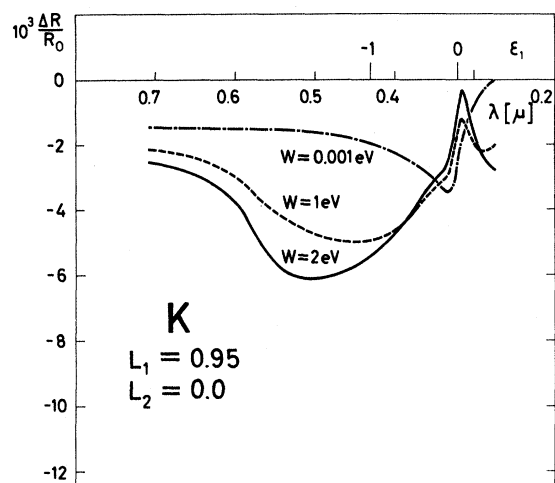


FIG. 3. Calculated relative change in the reflectivity  $\Delta R/R_0$  for potassium plotted vs wavelength for three values of  $W$ . The depolarization factors  $L_1$  and  $L_2$  are typical of a well-annealed sample and  $V_f=0.01$ .

with  $L_1$  and  $L_2$  characteristic of 500-Å grain size in Fig. 4 and 100-Å grain size in Fig. 5. In both cases the volume fraction of ellipsoids was nominally set to 0.01. Again there is a broad resonance in the region 0.35–0.60  $\mu$ , but now we see a second resonance emerge at 0.325  $\mu$ , i. e., just below the plasma frequency in potassium. The long-wavelength resonances shift towards shorter wavelengths as  $L_1$  is decreased and  $L_2$  is increased. The short-wavelength resonances shift in the opposite direction.

The nature of these resonances is easy to under-

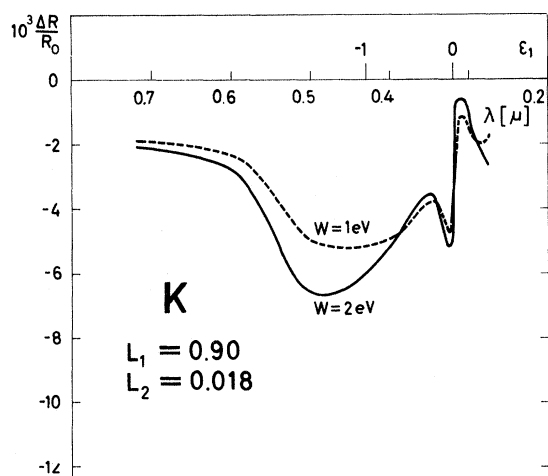


FIG. 4. Calculated relative change in the reflectivity  $\Delta R/R_0$  for potassium plotted vs wavelength for two values of  $W$ . The depolarization factors  $L_1$  and  $L_2$  are typical of 500-Å grains and  $V_f=0.01$ .

TABLE I. The error in  $1-R_0$  due to a fractional volume 0.01 of grain boundaries for one wavelength near resonance and one wavelength well below resonance.

K $W=1$ eV		Ag $W=2$ eV		Au $W=2$ eV	
$\lambda$ ( $\mu$ )	$\frac{\Delta R}{1-R_0}$ ( $10^{-2}$ )	$\lambda$ ( $\mu$ )	$\frac{\Delta R}{1-R_0}$ ( $10^{-2}$ )	$\lambda$ ( $\mu$ )	$\frac{\Delta R}{1-R_0}$ ( $10^{-2}$ )
0.45	5.5	0.40	7.6	0.58	2.2
0.70	6.2	0.80	3.5	0.80	4.9

stand. Assume at first  $L_1=1$ ,  $L_2=0$ . This corresponds to a thin parallel slab of grain-boundary material embedded in the sample normally to the surface. As is well known,<sup>9</sup> a component of the electric field normal to the surface of a very thin slab will excite a plasma oscillation in the slab when  $\omega = \omega_p^b$ —the bulk-plasmon frequency of the material in the slab, irrespective of the dielectric constant of the surrounding medium. When  $L_1 \neq 1$  the resonance condition depends upon the surrounding medium, but the nature of the resonance is essentially unchanged. Both resonances in Figs. 3–5 are plasma resonances excited by light polarized along the two main axes of the ellipsoids parallel to the surface, respectively. The positions of the resonances are remarkably insensitive to the shape of the ellipsoids.

When  $R_0$  approaches unity,  $\epsilon_2$  is proportional to  $1-R_0$ . The error in  $1-R_0$  due to a fractional volume 0.01 of grain boundaries is given in Table I.  $V_f=0.01$  was what one found for a typical well-annealed gold film by direct measurement. The error in  $1-R_0$  and thus in  $\epsilon_2$  is not negligible. If one increased the lifetime of electrons near the grain boundaries the error far away from the plasma res-

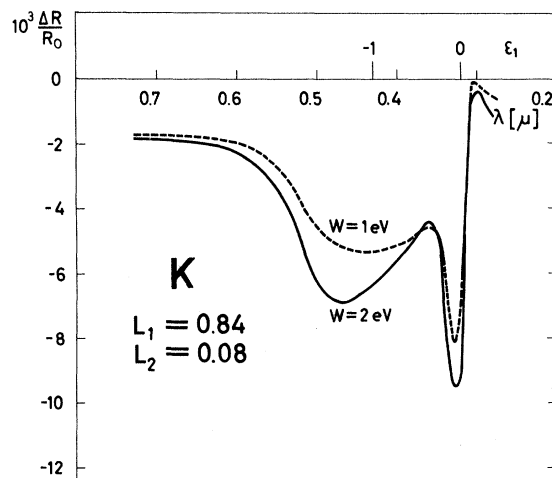


FIG. 5. Calculated relative change in the reflectivity  $\Delta R/R_0$  for potassium plotted vs wavelength for two values of  $W$ . The depolarization factors  $L_1$  and  $L_2$  are typical of 100-Å grains and  $V_f=0.01$ .

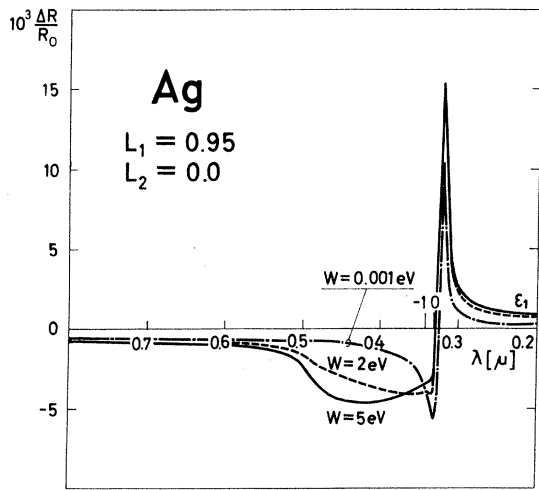


FIG. 6. Calculated relative change in the reflectivity  $\Delta R/R_0$  for silver plotted vs wavelength for three values of  $W$ . The depolarization factors  $L_1$  and  $L_2$  are typical of a well-annealed sample and  $V_f=0.01$ .

onances would decrease but the error at resonance would increase. Decreasing  $W$  decreases the error at resonance. However, there is reason to believe that even in well-annealed samples, relatively large variations in the electron density near the grain boundary may still occur (see Sec. V). Unfortunately, the maximum change in  $\epsilon_2$  occurs in the interband region of potassium and may easily be mistaken for interband structure. One concludes that the minimum grain size necessary to give bulk conditions, defined as an error in  $\epsilon_2$  of less than 1%, is about  $1.2 \mu$ .

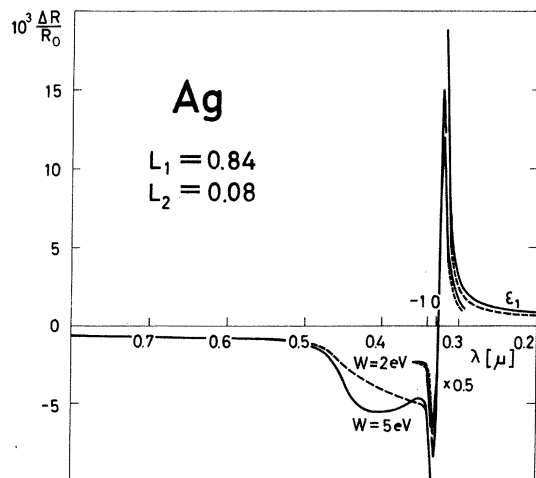


FIG. 7. Calculated relative change in the reflectivity  $\Delta R/R_0$  for silver plotted vs wavelength for two values of  $W$ . The depolarization factors  $L_1$  and  $L_2$  are typical of 100-Å grains and  $V_f=0.01$ .

### B. Noble Metals

Figure 6 shows the relative change in reflectivity,  $\Delta R/R_0$ , for a silver sample as a function of wavelength for different values of the parameter  $W$ . The parameters  $L_1$  and  $L_2$  are characteristic of a well-annealed sample (grain diameter  $> 0.2 \mu$ ). The volume fraction has again nominally been set to 0.01. For the dielectric constant of the noble metals the values obtained by Beaglehole and Erlbach<sup>10</sup> were used. The results are similar to those found in potassium. We observe plasma resonances—a broad structure in the visible and near uv for the two values of  $W \neq 0$  with an additional weak structure at  $0.335 \mu$ , just below the plasma frequency  $\omega_p$  in silver. For  $W=0$  the only structure is at  $0.335 \mu$ .  $\Delta R/R_0$  changes sign in silver. This happens near the interband edge where  $dR/d\epsilon_2$  changes sign from negative to positive. The sharp positive structure at  $0.320 \mu$  arises from the division by  $R_0$ .

When  $L_2$  becomes finite a second resonance emerges below  $\omega_p$  just as for potassium. This is shown in Fig. 7 where  $\Delta R/R_0$  is plotted as a function of wavelength with  $L_1$  and  $L_2$  characteristic of 100-Å grain size and with  $V_f=0.01$ . As in potassium we see that the position of the resonances is not very sensitive to the shape of the ellipsoids. For  $W=1 \text{ eV}$  one finds two peaks if  $\Delta R$  is plotted instead of  $\Delta R/R_0$ .

In Figs. 8 and 9 the relative change in reflectivity in gold due to grain boundaries is plotted for the same set of parameters as in Figs. 6 and 7 above. The plasmons are strongly damped in the interband region in gold and the maximum change occurs just

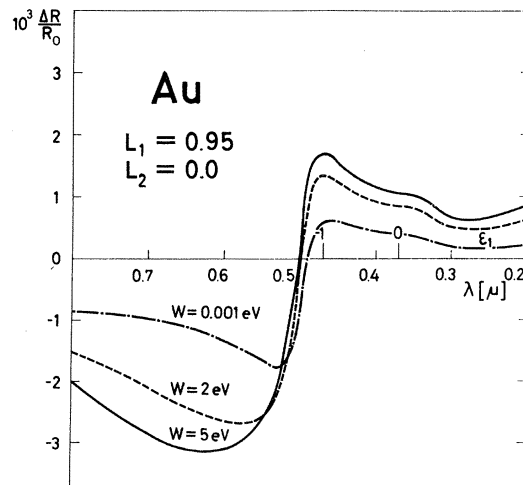


FIG. 8. Calculated relative change in the reflectivity  $\Delta R/R_0$  for gold plotted vs wavelength for three values of  $W$ . The depolarization factors  $L_1$  and  $L_2$  are typical of a well-annealed sample and  $V_f=0.01$ .

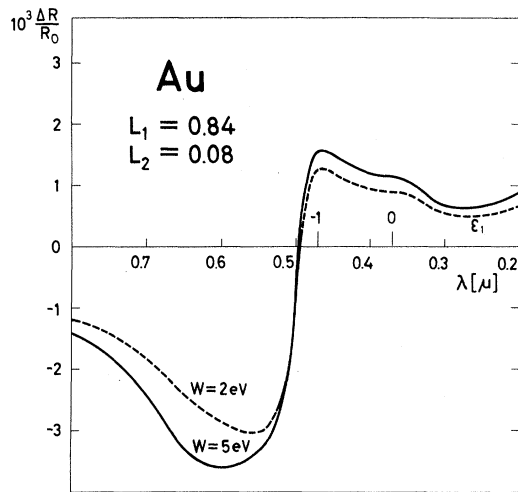


FIG. 9. Calculated relative change in the reflectivity  $\Delta R/R_0$  for gold plotted vs wavelength for two values of  $W$ . The depolarization factors are typical of 100-Å grains and  $V_f=0.01$ .

below the interband edge.  $\Delta R/R_0$  changes sign at the interband edge as in silver, when  $dR/d\epsilon_2$  changes sign. Since the calculations only take the change of the Drude part into account, the results in the interband region are of limited validity. A local change in the electron density will also lead to a change in the interband part of  $\epsilon$ . That, however, is outside the scope of these calculations.

From Figs. 6-9, the minimum grain size necessary to give bulk conditions defined as above was estimated to be about  $1.5 \mu$  in silver and  $1.0 \mu$  in gold.

#### V. COMPARISON WITH OTHER WORK

In this section a few experimental observations reported in the literature which the author feels can be explained in terms of this model are discussed.

#### A. Alkali Metals

In a recent paper Palmer and Schnatterly<sup>8</sup> observed a large anomalous decrease in the reflectivity of potassium and sodium below the plasmon edge when the metals were evaporated onto a cold substrate. It disappeared when the samples were annealed at room temperature and did not reappear upon recooling. The anomalous absorption was attributed to the excitation of surface plasmons which coupled to the incident field via surface roughness. They concluded that the surface roughness disappeared during annealing. This is, however, contrary to the author's experience with silver.<sup>11</sup> There, annealing of the film at high temperatures ( $T=500^\circ\text{C}$ ) produces roughness instead of removing it.

To explain the Palmer-Schnatterly data required a rms surface roughness of  $50 \text{ \AA}$ . The scalar scattering theory then predicts a total nonspecular scattering of 1.6% at  $0.5 \mu$  and 2.5% at  $0.4 \mu$ .<sup>12</sup> In practice, the scattering would be even larger due to plasmon reradiation. This should be clearly observable with the eye. The calculations of a rms roughness of  $50 \text{ \AA}$  is very approximate, and the value could be a factor of 3 lower. This should still be discernible with a strong lamp, but no scattering was observed at all.

The same type of anomalous absorption has recently been observed by Hunderi and Myers<sup>13</sup> in silver films deposited onto cold substrates. Again no appreciable amount of nonspecularly reflected light was observed. Silver is well known to give smooth films at room temperature and the author sees no reason to expect a rough surface at lower temperatures. Furthermore, in silver the maximum anomalous absorption occurred at a frequency which was clearly separated from the surface plas-

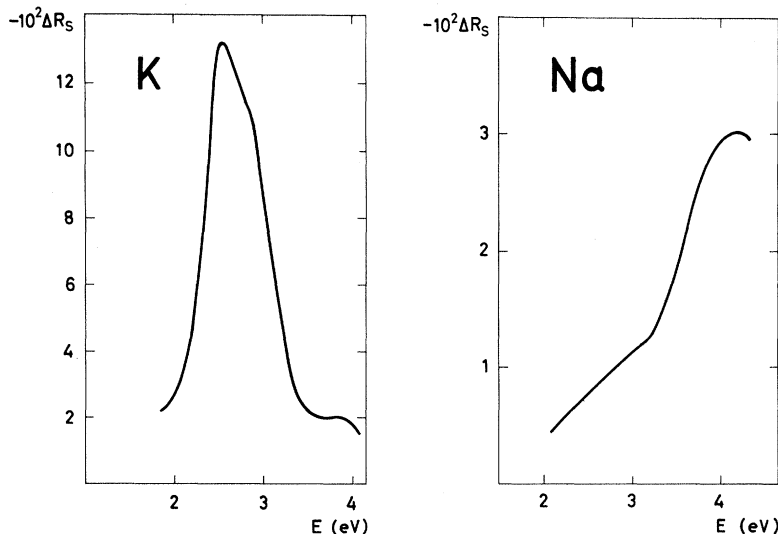


FIG. 10. Experimental change in the reflectivity of  $s$ -polarized light from annealing,  $\Delta R_s$ , plotted vs energy for potassium and sodium. The angle of incidence was  $45^\circ$  and the sample temperature was  $77 \text{ K}$  (after Palmer and Schnatterly, Ref. 8).

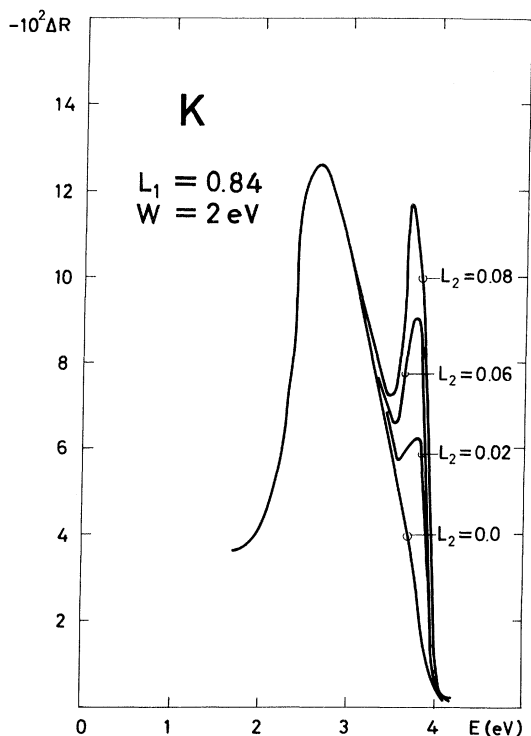


FIG. 11. Calculated change in reflectivity for potassium plotted vs energy. The depolarization factors  $L_1$  and  $L_2$  are typical of 100-Å grains and  $V_f=0.2$ .

mon frequency. One must therefore conclude that all these films were smooth.

When a film is deposited onto a cold substrate, the ion mobility is low and the average grain size is small. The fractional volume occupied by what has been termed grain-boundary material is large and the author believes that grain-boundary plasma resonances are responsible for the anomalous absorption in the alkali metals and in silver.

Palmer and Schnatterly measured the quantity  $N = (R_s - R_p)/(R_s + R_p)$  at a  $45^\circ$  angle of incidence. At this angle,  $R_p = R_s^2$  and  $N$  becomes  $(1 - R_s)/(1 + R_s)$ . The difference in reflectivity of  $s$ -polarized light between unannealed and annealed samples at 77 K,  $\Delta R_s$ , has been calculated from the published graphs. In Fig. 10 the resulting  $\Delta R_s$  is plotted versus wavelength. In the sodium data the annealing does not seem complete; this gives a shoulder on the  $\Delta R_s$  curve.

Figures 11 and 12 show  $\Delta R = R - R_0$  calculated from the above model for potassium and sodium, respectively. The potassium curves were calculated with the parameters  $L_1$  and  $V_f$  representative of an average grain size of 100 Å and for three different values of  $L_2$ . The sodium curve was calculated with parameters representative of 400-Å grains.

The line shapes of the experimental and calculated curves are very similar. The positions of the peaks are in excellent agreement with experiment. The experimental and theoretical half-widths of the peak in potassium are comparable, 0.4 and 0.6 eV, respectively. The total decrease predicted by the theory is also of the correct magnitude for the chosen parameters.

A fairly large value of the scattering parameter  $p$  was chosen in the calculations. A smaller value of  $p$  would increase the mean lifetime and hence decrease the imaginary part of the dielectric constant of the grain-boundary material. This would increase the plasma absorption and decrease the additional Drude background giving better agreement between the experimental and theoretical half-widths and predicting somewhat larger grain size. The experimental data do not go sufficiently far into the red to give information about the value of  $p$ .

The experiment measured  $\Delta R_s$  at a  $45^\circ$  angle of incidence while the calculations were for normally incident light. For that reason, and also since multiple-scattering effects become important for the volume fraction chosen, the peak values of  $\Delta R$  and  $\Delta R_s$  were not fitted more accurately. Note, however, that the positions of the peaks and the line shape will not depend upon the angle of incidence when  $R$  is large—only the magnitude will.

Palmer and Schnatterly observed additional structure in the absorption near 2.90 eV in potas-

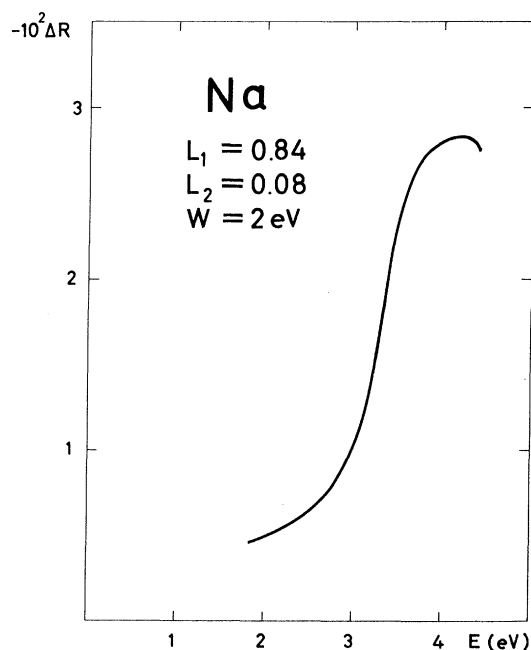


FIG. 12. Calculated change in reflectivity for sodium plotted vs energy. The depolarization factors  $L_1$  and  $L_2$  are typical of 400-Å grains and  $V_f=0.05$ .

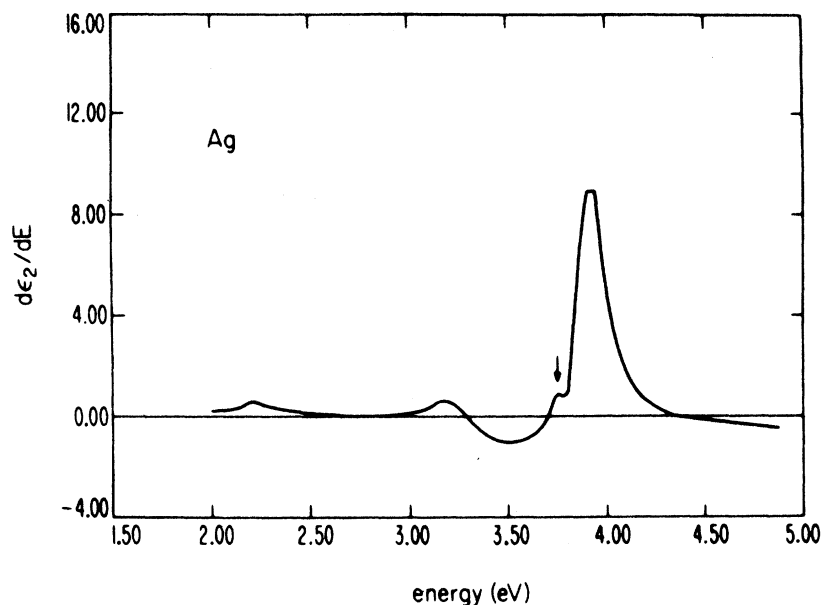


FIG. 13. Derivative of the imaginary part of the dielectric constant,  $d\epsilon_2/dE$ , at 77 K for silver plotted vs energy (after Welkowsky and Braunstein; Ref. 17).

sium and 4.1 eV in sodium. Density fluctuations will provide a coupling mechanism between surface plasmons and an electromagnetic wave.<sup>14</sup> Surface plasmons are excited when  $\epsilon_1 = -1$ . In potassium this happens at 2.9 eV and in sodium at 3.89 eV. This is close to where structure is observed and surface-plasmon excitation may account for the structure. In the present model this corresponds to magnetic-dipole terms, which would give additional structure to the peak if included in the calculations.

Recently, additional structure has also been observed in the plasmon absorption of *p*-polarized light incident on very thin films.<sup>15</sup> This is due to the excitation of longitudinal plasmons. Similar structure might also occur in the grain-boundary plasma resonances.

#### B. Silver

The general behavior of the reflectivity of silver predicted by Fig. 6 for  $W = 5$  eV is often observed experimentally. Even well-annealed films sometimes show a small decrease in the reflectivity in the region  $0.35\text{--}0.45 \mu$  with a subsequent increase for longer wavelengths.<sup>16</sup>

A very sensitive way to detect small structures in the reflectivity is wavelength-modulation spectroscopy. The non-Drude behavior of silver films has been studied in this way by Welkowsky and Braunstein.<sup>17</sup> Their result for the energy derivative of the imaginary part of the dielectric constant,  $d\epsilon_2/dE$ , is reproduced in Fig. 13. Three structures are observed in addition to the interband structure at 3.9 eV. One of these (at 3.3 eV) is a result of the interaction of light with surface

plasmons; the coupling mechanism being provided by surface roughness. Welkowsky and Braunstein suggested that the structure at 3.77 eV arose from the splitting of the interband edge in silver. This does not agree with recent measurements by Liljenwall and Mathewson,<sup>18</sup> who were able to separate the edges clearly by measuring  $\epsilon_2$  at different temperatures.

The structure in  $d\epsilon_2/dE$  at 2.25 and 3.77 eV can be interpreted as arising from grain-boundary plasma absorption. In Fig. 14,  $\Delta\epsilon_2$  from Eq. (12) is plotted with  $V_f c_f$  substituted by  $V_f \sum_i g_f^i \alpha_f^i$  and with  $L_1 = 0.95$  and  $L_2 = 0.025$ .  $V_f$  has nominally been set to 0.01. In the calculations there is an additional Drude background not included in the Welkowsky-Braunstein results. Subtracting the Drude background gave two maxima in  $d\epsilon_2/dE$ , one

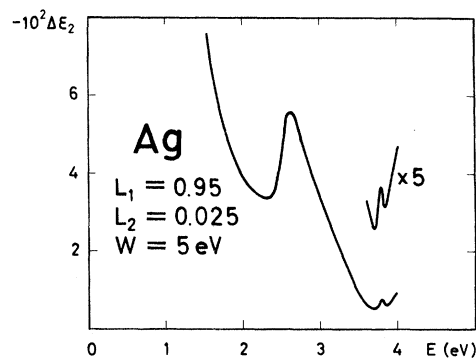


FIG. 14. Calculated change in the imaginary part of the dielectric constant for silver,  $\Delta\epsilon_2$ , plotted vs energy;  $V_f = 0.01$ .

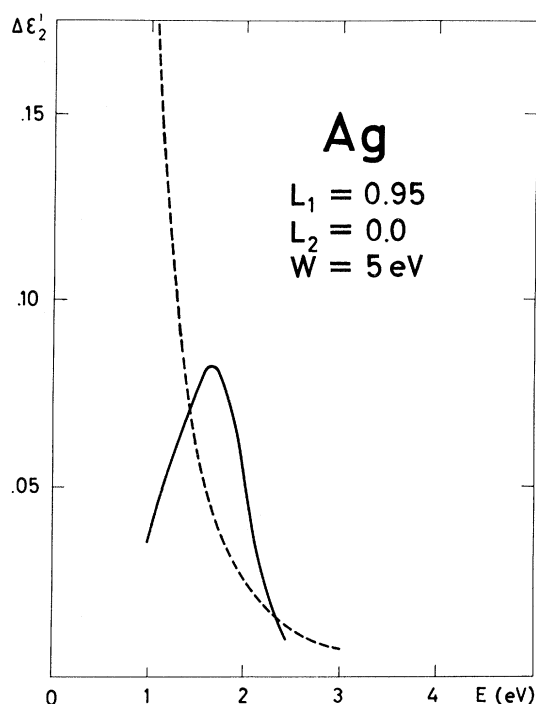


FIG. 15. Calculated change in the imaginary part of the dielectric constant for gold,  $\Delta\epsilon_2$ , divided into a Drude part (dashed line) and an anomalous-absorption part (solid line) plotted vs energy;  $V_f=0.01$ .

at 2.4 and one at 3.75 eV. The magnitude of  $d\epsilon_2/dE$  at 2.4 eV was  $0.16 \text{ eV}^{-1}$  for  $V_f=0.01$  and about five times less at 3.75 eV. Experimentally, the low-energy maximum in  $d\epsilon_2/dE$  was  $0.55 \text{ eV}^{-1}$ , so  $V_f=0.034$  gave the correct magnitude. The samples used in the experiment were evaporated onto substrates at room temperature but not annealed at higher temperatures, so  $V_f=0.034$  does not seem unreasonable.

Throughout these calculations the room-temperature values of the dielectric constants were used. It should be noted that the experiment was performed at 80 K and the value of  $V_f=0.034$  is therefore probably an overestimate. Decreasing the temperature decreases  $\epsilon_2$  both in the bulk and in the grain boundary and hence increases the grain-boundary resonance.

These results indicate that even in samples evap-

orated onto substrates at room temperature, large density variations may be found along the grain boundaries.

#### C. Gold

In poorly crystallized gold films an additional absorption band centered at 1.35 eV and of half-width 0.44 eV was observed by Devant and Theye.<sup>1</sup> This additional absorption band probably arises from plasma resonances along the grain boundaries. The change in  $\epsilon_2$  from such resonances was calculated using Eq. (12) with  $V_f\alpha_f$  substituted by  $V_f\sum_i g_f^i \alpha_f^i$ . The total change in  $\epsilon_2$  was split into a Drude part and an anomalous-absorption part. The result is shown in Fig. 15, where the two contributions to the change in  $\epsilon_2$  are plotted versus energy. We observe an additional absorption band centered at 1.6 eV and of half-width 0.5 eV. The predicted magnitude of the additional absorption is somewhat small, which shows that the original choice of the scattering parameter  $p=0.5$  was probably an overestimate.

#### VI. SUMMARY

This approach to the interaction of light with samples containing grain boundaries correctly predicts several experimental observations. The large value of  $W$  necessary to fit theory and experiment may seem unreasonable to some. A good description of the experimental facts could have been obtained with smaller values for  $W$  if the average electron density near the grain boundaries was smaller than the bulk density. Experimental observations in this laboratory<sup>13</sup> (Chalmers University of Technology) indicate that this may be the case. The observed plasmon frequency in samples with small grains are found to be much smaller than the plasmon frequency in well-annealed samples.

#### ACKNOWLEDGMENTS

The author wishes to thank Professor David Beaglehole for suggesting the problem and for many helpful discussions. He also wishes to express his gratitude to the The Norwegian Research Council NAVF for partial support while at Chalmers University of Technology, and Professor H. Peter Myers for valuable comments on the manuscript.

\*Present address: Physics Department, Chalmers University of Technology, Gothenburg, Sweden.

<sup>1</sup>G. Devant and M. L. Theye, Proceedings of the Second Colloquium on Thin Films, Budapest, 1967 (unpublished).

<sup>2</sup>H. Gleiter, Phys. Status Solidi **45**, 9 (1971).

<sup>3</sup>F. L. Galeener, Phys. Rev. Lett. **27**, 1716 (1971).

<sup>4</sup>O. Hunderi and D. Beaglehole, Phys. Rev. B **2**, 321 (1970).

<sup>5</sup>H. C. Van der Hulst, *Light Scattering by Small Particles*

(Wiley, New York, 1957).

<sup>6</sup>R. W. Sillars, J. Inst. Electr. Eng. **80**, 378 (1937).

<sup>7</sup>D. Polder and J. H. van Santen, Physica **12**, 257 (1946).

<sup>8</sup>R. E. Palmer and S. E. Schnatterly, Phys. Rev. B **4**, 2329 (1971).

<sup>9</sup>A. J. McAllister and E. A. Stern, Phys. Rev. **132**, 1599 (1963).

<sup>10</sup>D. Beaglehole and E. Erlbach (private communication).

- <sup>11</sup>D. Beaglehole and O. Hunderi, Phys. Rev. B **2**, 309 (1970).  
<sup>12</sup>H. Davis, Proc. Inst. Electr. Eng. **101**, 209 (1954).  
<sup>13</sup>O. Hunderi and H. P. Myers, J. Phys. F (to be published).  
<sup>14</sup>R. K. Ritchie and R. E. Wilems, Phys. Rev. **178**, 372 (1969).  
<sup>15</sup>I. Lindau and P. O. Nilsson, Phys. Lett. **31A**, 352 (1970).  
<sup>16</sup>D. Beaglehole (private communication).  
<sup>17</sup>M. Welkowsky and R. Braunstein, Solid State Commun. **9**, 2139 (1971).  
<sup>18</sup>H. G. Liljenwall and A. G. Mathewson, J. Phys. C Suppl. **3**, 341 (1970).

PHYSICAL REVIEW B

VOLUME 7, NUMBER 8

15 APRIL 1973

## Energy-Level Structure of Zinc in Magnetic Fields Using a Single-Band Effective Hamiltonian

P. S. Kapo\* and E. Brown

*Rensselaer Polytechnic Institute, Troy, New York 12181*

(Received 17 July 1972)

The zero-magnetic-field energy-band structure of the midplane of the second band of zinc is Fourier analyzed and the coefficients  $\mathcal{E}(\vec{R})$  are used to construct the magnetic effective Hamiltonian  $H(\vec{\pi}) = \sum_{\vec{R}} \mathcal{E}(\vec{R}) \exp(i\vec{R} \cdot \vec{\pi}/\hbar)$  ( $\vec{\pi} = \vec{p} + e\vec{A}/c$ ). This effective Hamiltonian is cast into the form of a matrix operator, and the eigenvalues are computed by numerical means for a range of magnetic fields. These exact solutions of the effective Hamiltonian display characteristics which can be compared with semiclassical results. The energy levels of the effective Hamiltonian form bands in a "magnetic zone" which is a zone in reciprocal space much smaller than the Brillouin zone. Within a magnetic zone the wave function and energy are functions of a vector  $\vec{q}$  which is in many respects similar to the zero-field wave vector  $\vec{k}$ . These magnetic bands can be associated with Landau levels corresponding to circular, lens, or triangle shaped contours, and as the magnetic field is varied the energies of the magnetic bands evolve in the manner that Landau levels are predicted to evolve from semiclassical arguments. The spacing of lens and triangle bands confirms the Onsager rule of equal areas between Landau contours; however, a systematic deviation is noted, the maximum deviation being about 5%. The Roth correction to the Onsager rule roughly predicts this deviation. The bands associated with lens and triangle contours display considerable broadening indicating strong coupling between these orbits.

### INTRODUCTION

The problem of determining the energy-level structure of an electron in a periodic potential with a superimposed magnetic field is readily treated in terms of an effective Hamiltonian. The validity of such an approach is now well established.<sup>1-6</sup> A useful simplification of the problem can be obtained by making use of the fact that the Hamiltonian is invariant under a set of operations known as magnetic translations.<sup>5,6</sup> By means of group-representation theory it is possible to determine the symmetry properties and degeneracies of magnetic energy levels. By means of this group-theoretical method it is possible to construct the magnetic analog of Wannier functions from which it is a simple matter to prove the validity of a one-band effective Hamiltonian, the form of which depends on the magnetic field.

Using this scheme, Butler<sup>7</sup> considered a tight-binding form of a single-band effective Hamiltonian and used accurate numerical procedures to obtain a detailed level structure.

The present paper is an extension of the method used by Butler to a model effective Hamiltonian that approximates a real metal. Specifically an ef-

fective Hamiltonian is constructed which simulates the midplane of the second band in zinc with the magnetic field along the hexagonal axis. This section of the band and field orientation were chosen because it is considered likely that magnetic breakdown occurs here. This phenomenon has been of interest for some time.<sup>8-14</sup> In order to apply the effective-Hamiltonian method to this problem properly it would be necessary to use a multiband formalism including the second and third bands. As a preliminary to such a calculation it was considered worthwhile to investigate a single-band model effective Hamiltonian in some detail. An extension of this work based on a two-band formalism has recently been carried out by Zablottney.<sup>15</sup>

Briefly the procedure is as follows: The zero-field band is mapped using the nearly-free-electron approximation. A sufficient number of Fourier coefficients are calculated for the truncated Fourier series to give a reasonably good fit to this energy band. The magnetic effective Hamiltonian is constructed using these coefficients.<sup>16</sup> Exact numerical calculations of the magnetic level structure for this portion of the energy band are carried out for a range of magnetic fields. This level structure is